Research Square

Preprints are preliminary reports that have not undergone peer review.
They should not be considered conclusive, used to inform clinical practice,
or referenced by the media as validated information.

Deep-Learning Based ECG-free Heart-Carotid Pulse Transit Time Estimation from Laser Doppler Vibrometry

Simeon Beeckman

simeon.beeckman@ugent.be

Ghent University

Smriti Badhwar

INSERM U970

Rosa Maria Bruno

INSERM U970

Yanlu Li

Ghent University-imec

Soren Aasmul

Medtronic

Silvia Seoni

Politecnico di Torino

Patrick Segers

Ghent University

Nilesh Madhu

Ghent University

Article

Keywords: Heart-carotid pulse transit time, Laser Doppler vibrometry, Electrocardiography, Deep learning, Template Matching

Posted Date: July 29th, 2026

DOI: https://doi.org/10.21203/rs.3.rs-7881056/v1

License: This work is licensed under a Creative Commons Attribution 4.0 International License.
Read Full License

Additional Declarations: No competing interests reported.

Deep-Learning Based ECG-free Heart-Carotid Pulse Transit Time Estimation from Laser Doppler Vibrometry

Simeon Beeckman[1], Smriti Badhwar[2], Rosa Maria Bruno[2,3], Yanlu Li[4], Soren Aasmul[5], Silvia Seoni[6], Patrick Segers[1], Nilesh Madhu[7]

[1]IBiTech-BioMMedA, Ghent University, Ghent, 9000, Belgium.
[2]Paris Cardiovascular Research Center, INSERM U970, Paris, 75015, France.
[3]Assistance Publique – Hôpitaux de Paris, Paris, 75610, France.
[4]Photonics Research Group, Ghent University-imec, Technologiepark-Zwijnaarde 126 Ghent, 9052, Belgium.
[5]Bakken Research Center, Medtronic, Ghent, 9000, Belgium.
[6]PolitoBIOMed Lab, Biolab, Politecnico di Torino, Turin, 10129, Italy.
[7]IDLab, Ghent University, Ghent, 9052, Belgium.

Contributing authors: simeon.beeckman@ugent.be; smriti.badhwar@inserm.fr; rosa-maria.bruno@inserm.fr; yanlu.li@ugent.be; soren.aasmul@medtronic.com; silvia.seoni@polito.it; patrick.segers@ugent.be; nilesh.madhu@ugent.be;

Abstract

Assessment of arterial stiffness is important in the diagnosis and management of cardiovascular diseases. A strong biomarker for arterial stiffness is pulse-wave velocity (PWV) – the speed at which a heartbeat-induced pulse wave travels through the large arteries. By measuring the pulse-transit time (PTT) – the time delay between the arrival of the pulse wave – at two points on the arterial pathway, PWV can be estimated. PTT can be calculated from skin-displacement signals, measured via laser Doppler vibrometry (LDV). This process requires an accurate indication of heartbeat onsets, to be able to utilize the correct signal features or fiducial points that lead to PTT. Typically, electrocardiography (ECG) is a reliable, parallel measurement to segment LDV signals. However, common practice for LDV does not include ECG due to increased measurement

time and complexity, necessitating alternative means for identifying heartbeat cycles from LDV signals. A proposed solution is a deep neural network (DNN) which returns an ECG-proxy for each LDV signal, containing information on the timing of the heartbeats. Heart-carotid PTT can then be calculated after segmenting the signals based on the predicted heartbeat timing. This PTT was additionally calculated via two other techniques i.e. a state-of-the-art template matching algorithm and a reference technique in which PTT was calculated via manual inspection of the data. The DNN was able to correctly predict the onset of 68% and 77% of heartbeats present in the test and validation sets respectively. When applied to unseen data of 100 subjects (45 female), it provided PTT values for 64 subjects that correlated well with the reference ($\boldsymbol{\rho = 0.71}$). In comparison, a state-of-the-art knowledge-driven approach yielded a similar correlation ($\boldsymbol{\rho = 0.69}$) but was only able to return PTT values for 46 subjects. An ECG-based ground truth method reached a correlation of $\boldsymbol{\rho = 0.69}$ for 90 subjects. Finally, the technique and rationale used for the DNN training demonstrates potential for broader biomedical LDV applications beyond heart-carotid PTT.

Keywords: Heart-carotid pulse transit time, Laser Doppler vibrometry, Electrocardiography, Deep learning, Template Matching

1 INTRODUCTION

The large arteries, particularly the aorta, play a crucial role in blood circulation [1]. Their structural properties enable the vessel wall to distend during cardiac contraction, storing elastic energy that is subsequently released during relaxation to maintain blood flow after the pressure wave has passed [1–3]. This mechanism ensures a near-continuous flow further along the arterial system, supporting constant organ perfusion. However, this buffering or 'windkessel' function deteriorates significantly when large arteries stiffen due to arteriosclerosis, resulting in dysregulated blood pressure, altered blood flow, and subsequent organ damage [4–7]. Understanding the shape and content of blood pressure and flow-related signals is essential for detecting and preventing early vascular aging as well as other related cardiovascular diseases (CVD), as CVD risk increases with an increase in large artery stiffness [5, 8, 9].

Common practice for the assessment of arterial stiffness is via the speed of the pressure wave which travels through the arterial tree following heart contractions [6, 10, 11]. This pulse-wave velocity (PWV) increases with increased stiffness. By measuring the distance dx between two measurement sites, and the time delay between the arrival of the pressure wave at these sites (i.e., the pulse transit time – PTT), the PWV is obtained as:

$$PWV = \frac{dx}{PTT} \tag{1}$$

Current state-of-the-art for measuring PWV is through applanation tonometry, magnetic resonance or ultrasound applied to the carotid and femoral arteries [10, 12–15]. These methods, while reliable, have a number of challenges associated with them: (i) they require specialized operator training, (ii) they are typically located

at dedicated medical facilities or hospitals, (iii) they can be expensive to acquire and (iv) there is a widely held consensus in the medical community that none of the aforementioned diagnostic methods can effectively identify a significant portion of at-risk individuals, both in primary care and secondary prevention settings [16]. Furthermore, individuals classified as low or moderate risk may remain undiagnosed.

As such, there is an interest in developing optimal diagnosis methods to institute a *timely* preventative therapy among those that are currently considered to be at low or moderate risk. Within the InSiDe consortium, we have been investigating laser-Doppler vibrometry (LDV) as an alternative technology to address these challenges [17–20]. LDV measures skin displacement at the location of large subcutaneous arteries such as the carotid and the femoral. By differentiating the displacement signal twice, skin acceleration is obtained. From these data, PTT can be estimated [21, 22]. It was demonstrated that these PTT and their corresponding PWV values strongly correlate with tonometry [23, 24].

The LDV prototype employed in this study was developed within the framework of the H2020 CARDIS project (Grant Agreement ID: 644798). The system consists of two handpieces (Figure 1), each equipped with six integrated laser beams operating at a wavelength of 1550 nm. The beams are arranged with an inter-beam spacing of 5 mm and are directed at the skin surface of the measurement site. To enhance signal quality, retroreflective tape was applied to the skin, thereby ensuring sufficient backscattered light for detection. A detailed technical description of the device has been reported in several previous works [22, 25, 26].

Multiple arterial pathways can be employed for the estimation of PTT, which may serve as additional biomarkers for the assessment of large artery stiffness and the risk prediction of associated cardiovascular disease (CVD). Among these, the heart–carotid pathway is of particular interest. In this case, PTT is calculated along a segment extending from the aortic valve at the base of the heart, over the ascending aorta, to the right common carotid artery [27, 28]. Our previous study has demonstrated correlations between heart–carotid PTT and established predictors of arterial stiffness, including chronological age and blood pressure. This was done for a clinical cohort of 100 CVD patients [29]. Figure 1 illustrates the heart–carotid measurement configuration and highlights the arterial segment under investigation.

In earlier investigations, heart–carotid PTT values were estimated manually through visual inspection of the recorded signals and using ECG to identify the onset of systole [29]. Manual estimations require time and expertise, making them unsuited for any potential LDV-procedures aimed at first-line medical practitioners. In contrast, this study seeks to advance the development of *automated* approaches for heart–carotid PTT estimation, thereby reducing reliance on manual interpretation and improving the feasibility of clinical deployment. In the remainder of this manuscript, the term pulse transit time (PTT) refers specifically to the heart–carotid PTT.

Manual PTT estimation formed the reference for evaluating automated estimation methods. This manual approach required the simultaneous acquisition of ECG alongside LDV recordings [29]. Proper segmentation allows for good PTT estimation. The ECG traces allowed the LDV signals to be segmented into individual cardiac cycles

(epochs), thereby simplifying the identification and alignment of fiducial points necessary for PTT calculation i.e. the carotid dicrotic notch and the onset of the second heartsound, see Figure 2.

Although effective, the requirement of parallel ECG recordings introduces practical challenges: incorporating the placement of ECG electrodes complicates the LDV measurement procedure, reduces ease-of-use for clinical staff, and increases the time required for patient examinations. Consequently, ECG acquisition will not be included in a commercially viable LDV-based medical device and is also not foreseen in future versions of the prototype.

For LDV to evolve into a viable technology for arterial stiffness assessment, it must nevertheless enable accurate and fully automated PTT estimation even in the absence of the ECG trace. To this end, this work presents a proxy for ECG, leading to robust LDV signal segmentation.

Alternative ECG-free approaches such as similarity-search or pattern-recognition techniques, including template matching (TM) [30–32] and matrix profile analysis [33], have been proposed. However, TM requires a predefined template, while matrix profiles may incorrectly identify unrelated recurring waveforms. Additionally, these methods are sensitive to signal quality, resulting in severe quality thresholds and consequent drop-out of a significant number of subjects [33, 34]. These shortcomings highlight the need for a robust approach capable of providing R-peak timing surrogates without parallel ECG acquisition or hand-crafted features and rigid analytical models associated with classical signal processing.

We propose a deep neural network (DNN) designed to map LDV signals to a proxy signal resembling ECG, thereby preserving cardiac gating information. Neural networks have been successfully applied to a broad range of biomedical signals, including seismocardiography (SCG) [35, 36], electrocardiography (ECG) [37, 38], electroencephalography (EEG) [39], magnetic resonance imaging (MRI) for aortic PWV estimation [40], and photoplethysmography (PPG) for the improvement of signal quality and derivation of PWV [41–44], among others [45–48]. Previously, PWV has also been directly estimated from cardiac risk factors using DNNs, but typically report high error rates or low agreement with measured PWV [49, 50]. To date, however, clinical LDV data have not been analyzed using neural networks.

To validate the proposed DNN-based automated PTT-estimation algorithm, we additionally implement an ECG-dependent and a template-matching method as benchmarks for the DNN-based approach. Because classical signal-processing methods such as TM are outperformed by DNNs in combining temporal context and learning non-linear relationships, we anticipate that (i) the DNN will provide a viable ECG proxy for signal segmentation, enabling automated PTT estimation in the absence of ECG; (ii) Following segmentation, calculated DNN-derived PTT values will correlate at least as strongly with the manual reference as those obtained via TM; and (iii) a larger fraction of subjects will yield reliable PTT estimates with the DNN-based approach compared to TM.

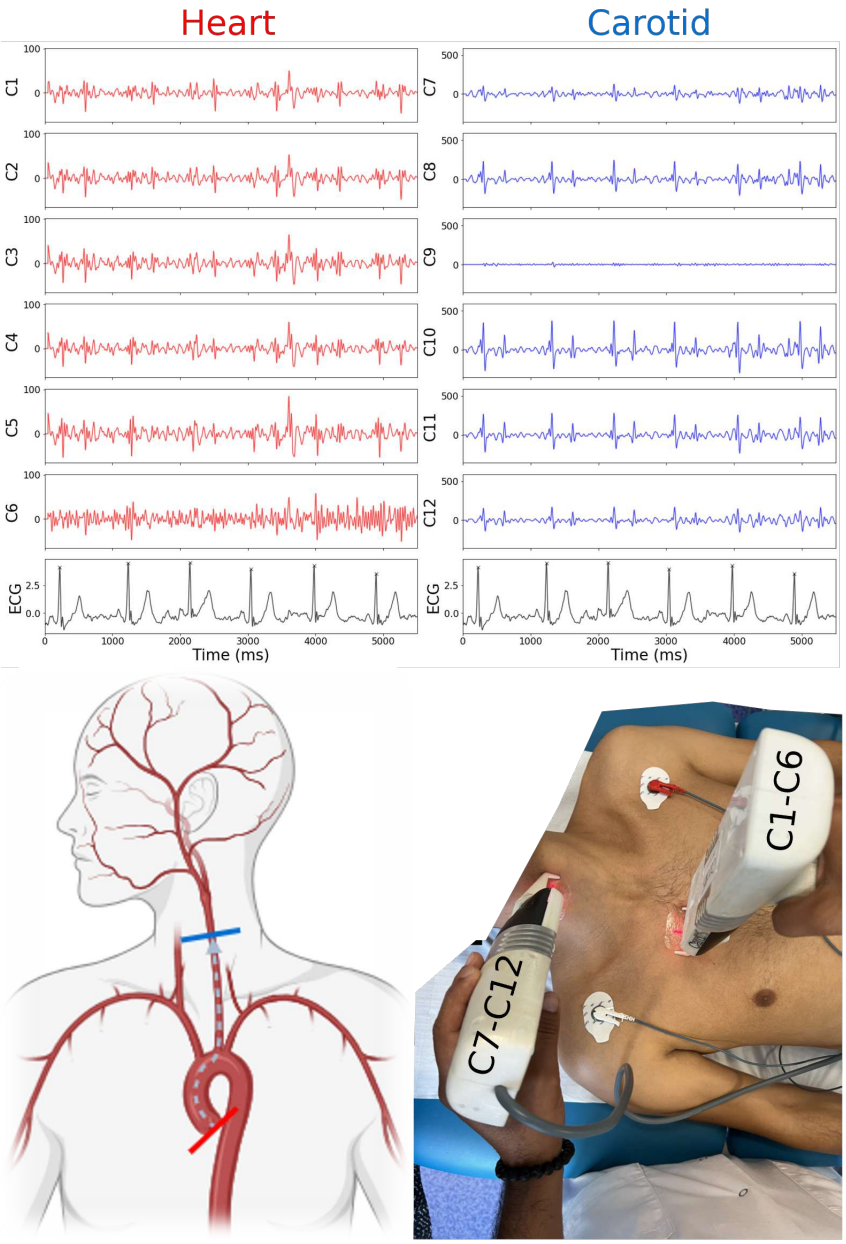


Fig. 1 Figure showing an example heart-carotid LDV measurement using the prototype handpieces. The top panel contains skin acceleration signals with the first column containing 6 heart signals (channel 1 = C1, etc.) and the second one the 6 carotid signals. Each handpiece contains 6 channels for a higher probability of at least one channel containing useful signal quality. The bottom row shows the ECG measured in parallel, to illustrate the rhythmic correspondence between ECG and LDV signals. The bottom-left panel sketches the anatomy of the considered arterial pathway. The bottom-right panel is a picture taken during the measurement, depicting the prototype as well as two ECG electrodes.

2 METHODS

The carotid and heart handpieces have $M = 6$ channels each as in Figure 1. For any handpiece, the LDV (discrete-time) acceleration signal at a channel $m \in \{1, 2, \ldots, M\}$ is modeled as:

$$x_m(n) = s_m(n) + v_m(n)\,, \tag{2}$$

where $s_m(n)$ is the underlying physiological signal *in channel* m and $v_m(n)$ is the noise in that channel. The accompanying ECG signal is denoted as ECG(n). Index n refers to the sample index with N being the total signal length in samples.

2.1 Applied principle for PTT calculation

All PTT calculation methods based on LDV signals for a given measurement have the same workflow:

1. Select the carotid and heart channels that will be used.
2. Partition each selected signal into separate heartbeats.
3. For each segment of every heart-carotid channel combination, combine fiducial points corresponding to the same heartbeat to estimate the PTT for that channel combination.
4. Calculate a final PTT value from all available PTT estimates by taking the median.

2.2 ECG based methods

First, an overview of the methods reliant on simultaneous ECG acquisition is provided. These methods serve as references to benchmark the automated methods.

2.2.1 Manual PTT estimate (reference method)

Manual heart-carotid PTT estimation served as an ECG-dependent ground truth to benchmark the automated PTT estimation algorithms. It was computed and evaluated in a previous study [29]. First, the channel with the highest signal quality was selected per handpiece based on visual inspection of the measurement data. Using the timing provided by the R-waves in the ECG(n), the selected LDV signals were segmented according to separate heartbeats or *epochs*. This simplified the search for and combination of corresponding fiducial points in both carotid and heart LDV signals for PTT estimation [29].

The physiological event underlying the relevant fiducial points in carotid and heart LDV signals is the aortic valve closure (AC). This event is associated with a region of elevated signal energy typically referred to as the second heartsound (S2). The fiducial point in the heart signal is then taken as the first perturbation before the minimum value during S2. The carotid fiducial point is taken as the second distinct peak in the carotid epoch, a.k.a. the carotid dicrotic notch (DN). This signal feature also corresponds to AC. a PTT estimate is then calculated from the time difference between heart and carotid fiducial points, as illustrated in Figure 2.

Five cardiac cycles were processed per measurement into five PTT estimations. These were selected based on their cross-correlation value with the average epoch of

the selected channel. The final manually determined PTT value was computed as the median of the single-cycle estimates.

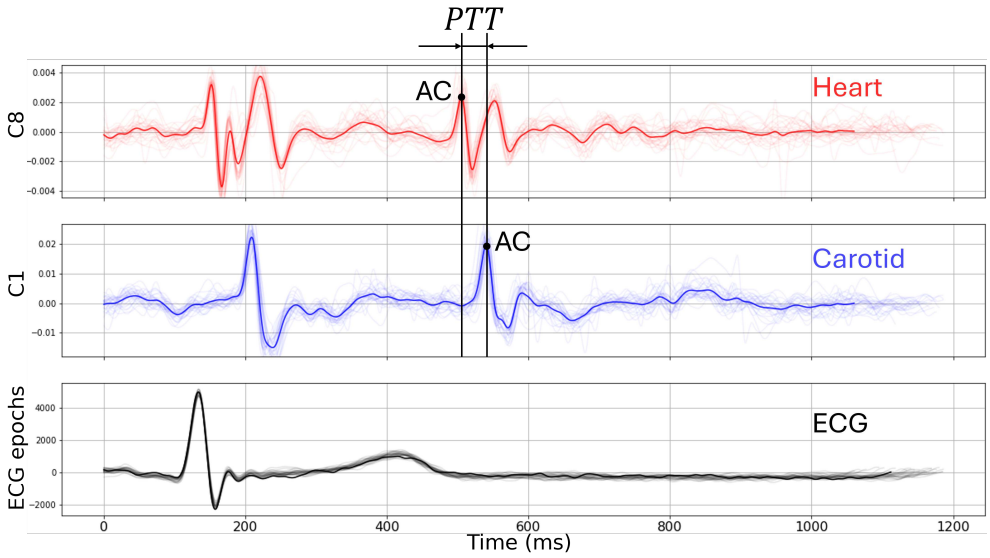


Fig. 2 Example of an ECG-based heartbeat segmentation of a carotid and heart channel combination (channel numbers 1 and 8). The top graph displays LDV-heart epochs of which one is highlighted. The middle graph shows the same for the carotid site. Fiducial points that were used to identify the timing of the closure of the aortic valve (AC) are indicated. PTT is calculated from a combination of the indicated heart and carotid fiducial points. The bottom graph contains individual epochs of the $ECG(n)$ signal that was used for LDV-signal segmentation.

2.2.2 ECG-based segmentation for automated PTT estimation

To verify the usefulness of DNN-based segmentation it was compared to the best possible segmentation information i.e. the heartbeat itself. Hence, as baseline, an experiment was conducted wherein PTT values were calculated on data that was segmented into separate heartbeats (or *epochs*) delineated by the I available R peaks in ECG(n).

As intra-subject signal quality can vary significantly between channels of one handpiece, a criterion was designed to remove channels with poor signal quality [33]. First, a signal-to-noise-ratio (SNR) estimate was computed as follows. The input signal power at channel m was obtained as:

$$P_{x,m} = \sum x_m^2(n)\,, \tag{3}$$

which represents the joint power of the target signal and noise. A median-filtered version of the input signal was next computed using a (non-causal) window of 5

samples:

$$\tilde{x}_m(n) \quad = \quad \text{median}(x_m(n\ -\ 2), x_m(n\ -\ 1), x_m(n), x_m(n\ +\ 1), x_m(n\ +\ 2)) \quad (4)$$

Noise was then approximated as $v_m(n) = x_m(n) - \tilde{x_m}(n)$ and its power was estimated:

$$P_{v,m} = \sum v_m^2(n) \quad (5)$$

Thereby, the SNR was estimated as:

$$\text{SNR}_m = \frac{P_{x,m}}{P_{v,m}} - 1 = \frac{P_{s,m}}{P_{v,m}} \quad (6)$$

SNR_m was calculated for all m channels per handpiece. Channels whose SNR_m deviated from the maximum value SNR_m value by more than one standard deviation were excluded from the analysis. The remaining carotid and heart channels were combined pair-wise for PTT estimation.

Every channel combination has segments corresponding to the I epochs in the ECG. While PTT was calculated on the same fiducial points as the reference (manual) PTT method, as in Figure 2, the key difference however was that the fiducial point detection was done in an automated manner. The carotid dicrotic notch was identified by taking the point of maximum acceleration within a window of 300 to 550 ms in the epochs of the selected carotid channel. The fiducial point corresponding to the aortic valve closure in the heart epochs was taken as the first peak before the absolute minimum within a window of 250 to 500 ms in heart channel epochs. The values of these windows were set based on the time between closure of the mitral valve (corresponding to the timepoint of the associated R-peak in ECG) and the closure of the aortic valve. This varies between 250-300 ms for healthy individuals, but can be elongated due to aging or disease [51, 52].

Assuming there are a total of J combinations of LDV segments yielding a plausible PTT value, PTT_j were then calculated for each valid beat. Only PTT values within a physiological range (5 ms to 60 ms) were considered valid, and the median of these values was used as the representative PTT for the recording, as in (7):

$$PTT = \text{median}(\boldsymbol{PTT})\,, \quad (7)$$

with $\boldsymbol{PTT} = \left[\text{PTT}_1, \text{PTT}_2, \ldots, \text{PTT}_J\right]^T$.

The final PTT was rejected if the total number of PTT estimates J was smaller than or equal to an empirically determined threshold of 15. This threshold was applied independently of the signal duration and served to filter out recordings with extremely poor signal quality. In such cases, the limited number of PTT estimates typically arose from the erroneous combination of random, noise-dominated waveforms rather than from the detection of physiologically meaningful features.

This method requires the additional ECG set-up which, as mentioned previously, is not foreseen for the clinical usage of LDV. Nevertheless, it serves as an upper performance bound for automated PTT estimation.

2.3 ECG-free methods

2.3.1 Template matching-based segmentation for automated PTT estimation

Without the ECG trace to identify heartbeat onsets and segment accordingly, the identification of required fiducial points is more challenging. One potential solution is a similarity-search algorithm based on *template matching* [33, 34].

The exact same signal-quality criterion as described in section 2.2.2, was applied to drop poor-quality channels. The remaining channels were assumed to be of sufficient quality and suited for template matching.

A template for the foot-of-the-wave waveform in carotid LDV acceleration signals was constructed as outlined in [33]. This waveform corresponds with a large peak in the acceleration signal, indicating the arrival of a pulse wave. For one heartbeat, two peaks are typically observed. The first one is referred to as the foot of the wave, while the second one corresponds to the dicrotic notch. The constructed template was cross-correlated with a sliding window on each considered carotid channel of the heart-carotid channel combination. A heartbeat onset was assumed when the normalized cross-correlation exceeded an empirically set threshold derived during a previous study ([33]).

For every detected beat, fiducial points corresponding to aortic valve closure were searched for in physiologically relevant windows. For the carotid DN, this window spanned between 250 and 500 ms after the detected heartbeat onset. The fiducial point in the heart signal, corresponding to aortic valve closure, lay within a window of 200 to 450 ms after the onset of the heartbeat. Similar to section 2.2.2, these windows were set with physiological cardiac timing and the construction of the template in mind. Indices at which template matching detects a beat are situated up to 50 ms later in time than the corresponding R-peaks [33].

In this way, *both* heart and carotid fiducial points depended on the template matching at the carotid level. The construction and application of a heart-signal template was deemed unsuitable due to the observed inter-subject variability in the heart-signal morphology. The carotid dicrotic notch was found as the maximum value in the carotid window. The aortic valve closure timing in the heart signal was taken as the first peak to the left of the minimum value in its respective window.

To ensure the quality of the resulting PTT values, a criterion was set on the variability in fiducial point timing. The method flagged the data as unreliable if either the timepoints at which the carotid DN was found, or the timepoints for the heart fiducial points had a standard deviation exceeding 60 ms. In these cases, the channel combination was dropped.

The final PTT values were calculated in the same way as in (7), employing the same criterion on the minimally accepted number of total PTT estimations made for a given measurement.

2.3.2 Data-Driven PTT Approach via DNN

Segmentation using ECG is beneficial. We want to realise this in the absence of the ECG signal. A DNN is used to generate a proxy for the ECG, based on the LDV signals.

This DNN was trained using z-normalized 4-second carotid LDV-signal segments as input. Each carotid channel m was segmented into K 4-second segments with 50% overlap. This returned e.g. for a signal of length 20 seconds, $K = 9$ overlapping segments. For every such LDV segment, the model provided an equally long output signal $\hat{E}'_{m,k}(n)$ of 4 seconds, with k the segment index. The individual output signals $\hat{E}'(n)$ were then concatenated using windowed overlap-add with perfect reconstruction condition [53], resulting in a model prediction $\hat{E}'_m(n)$ for carotid channel m.

The target signal to train the DNN had to be a signal from which segmentation of LDV signals into heartbeats was feasible. For our application, only the timing of R-peaks was needed, while ECG contains many more features that are not relevant for this work. Furthermore, the raw ECG signal, while rich in information, was deemed too complex to accurately predict with the available data. Hence, a transformation aimed at reducing complexity while conserving cardiac timing information was engineered first.

ECG-proxy as learning target

First, the ECG trace is replaced by a pulse train formed by Kronecker's delta functions at the location of the original R-peaks. Denote this as:

$$\mathrm{ECG}'(n) = \sum_i \delta(n - p_i)\,, \tag{8}$$

where p_i is the sample-index of the $i-$th R-peak. This does not yet suffice, however, as this pulse train is too sparse, which is not optimal for model training with the mean squared error (MSE) loss function.

Subsequently, this simplified ECG trace is convolved with a Gaussian filter, to yield the target signal $E'(n)$:

$$E'(n) = \mathrm{ECG}'(n) * g(n) = \sum_i g(n - p_i)\,, \tag{9}$$

where $g(n)$ is the Gaussian filter:

$$g(n) = \frac{1}{\sigma\sqrt{2\pi}} \exp\left(-\frac{n^2}{2\sigma^2}\right). \tag{10}$$

σ is the width of the kernel and a hyperparameter of this method. It was empirically set at $\sigma = 75$ samples. For an example segment k, the transformed signal is contrasted with the original trace in Figure 3.

For the model training, the mean-squared error (MSE) is calculated as:

$$\mathrm{MSE} = \frac{1}{N} \sum_n (E'_k(n) - \hat{E}'_{m,k}(n))^2 \tag{11}$$

The target signal $E'(n)$ contained in segment k is denoted as $E'_k(n)$. The model-output for segment k of channel m is $\hat{E}'_{m,k}(n)$. N is the length of the 4-second segment at index k of channel m. Because of a 1 kHz sampling rate, $N = 4000$ samples.

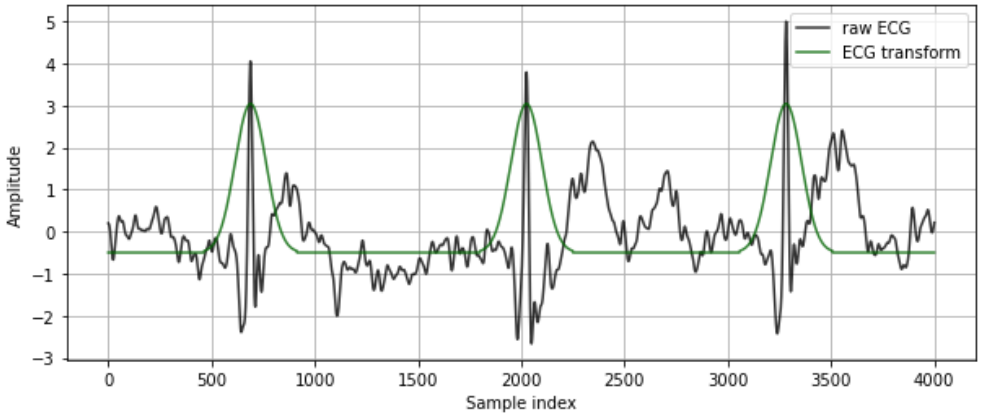


Fig. 3 Example of the transformation from raw ECG (ECG(n)) to the desired target signal ($E'(n)$), preserving the key timing features. This is illustrated for a randomly picked LDV segment. Data are z-normalized. $\sigma = 75$ samples.

DNN Structure and Training

We use a U-Net architecture for the proposed DNN. These architectures are widely used in biomedical image processing and have demonstrated their capacity for multi-scale feature extraction, end-to-end learning, and strong generalization from limited datasets [54]. A notable adaptation of U-Net to the one-dimensional time domain is Wave-U-Net , which leverages end-to-end learning to compute and combine features across different time scales for audio source separation.

We build upon the Wave-U-Net [55]. Our network has four convolutional layers in the encoder- and decoder blocks, and an added transformer layer in the bottleneck [56] for context-aware self attention. Each one-dimensional convolutional layer in the encoder and decoder is followed by batch normalization and a rectified linear unit (ReLU) activation function. Addition-based skip connections are employed to preserve feature continuity across scales. This architecture (Figure 4) is designed to retain both short- and long-term temporal dependencies, facilitating the learning of complex non-linear mappings between input and target signals. The model comprises approximately 25k learnable parameters.

During model training, the loss computed on the validation dataset was monitored to determine the optimal stopping point. Specifically, early stopping was applied by selecting the model configuration corresponding to the training epoch at which the validation loss ceased to improve for the following 50 epochs. The model was trained using the Adam optimizer with default hyperparameters, and the learning rate was fixed at 0.0001.

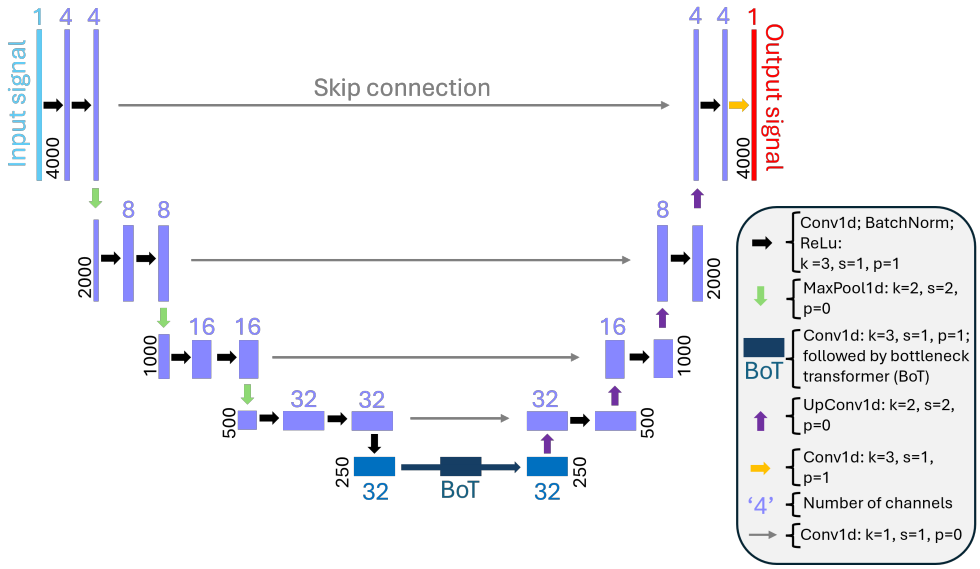


Fig. 4 Architecture of our DNN: each blue box represents a feature map with a number of channels equal to the number displayed on top of it. The 1D-data dimension is noted at the bottom of the relevant boxes. Arrows and notations corresponding to different operations are listed. k, s and p refer to kernel size, stride and padding respectively.

A cyclical batch size strategy was employed to the potential benefit for regularization and convergence [57]. The cycle length was set at 10 epochs, the minimum batch size at 2 and the maximum batch size at 64. The batch size followed a sinusoidal function.

In addition to the validation loss, model performance was assessed using an auxiliary metric, the R-peak score Q_R, calculated on each combination of 4-second model output segment $\hat{E}'_{m,k}(n)$ and its corresponding target signal $E'_k(n)$. This is the ratio of the number $(\hat{I})$ of R peaks detected in the output signal to the true number of R peaks (I) in the segment. A detected R-peak in the model output was considered correct if it occurred within a ± 30 ms window centered around the corresponding ground-truth R-peak:

$$Q_R = \frac{\hat{I}}{I} \tag{12}$$

To illustrate this, an example segment k for input, target and model output is presented in Figure 5. Peaks are found via simple peak-finding that has the criteria of a minimum amplitude $A_{min} = 1$ (all data is z-normalized) and with the additional constraint that the peaks should be separated by at least 500 ms to avoid detecting peaks in regions where an R-peak is physiologically improbable. A_{min} was found empirically. The 500 ms threshold restricts the method to subjects with a heart rate below 120 bpm, a criterion met by all participants in this study (see Table 1). Since LDV measurements are conducted at or near resting heart rates, the potential adverse impact of this threshold is minimal.

It should be noted that the example in Figure 5 was unseen data, and completely independent of the training set. For this specific segment, $Q_R = 100\%$. To monitor model performance throughout training, the mean Q_R was computed across all input datapoints in both the training and validation sets at each epoch.

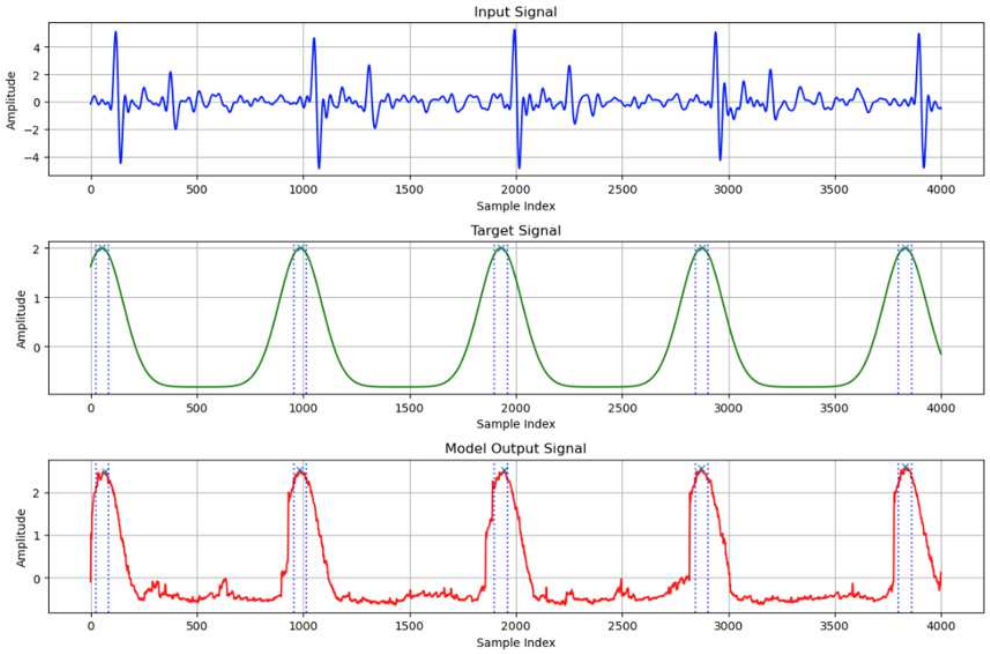


Fig. 5 Example of model prediction on segment k of unseen LDV data from a single channel m. The top graph shows the carotid-LDV segment that serves as model input. Its corresponding $E'_k(n)$ segment is displayed in the middle graph, and serves as target signal for this datapoint. The model prediction $\hat{E}'_{m,k}(n)$, is shown in the bottom plot. The vertical dotted lines indicate the tolerance window around target-signal peaks wherein output-signal peaks can lie for the prediction to be considered acceptable. Q_R in this case is 100%.

Application to PTT calculation

The DNN-based ECG-proxy estimate $\hat{E}'_m(n)$ is used to segment the LDV-signal $x_m(n)$ into separate heartbeats or epochs. In order to get to a PTT estimate, additional steps are required: starting from the $M = 6$ heart and carotid LDV channels for a given measurement, first a check on individual channel signal quality was implemented using SNR-based estimations. For the heart signals, SNR was calculated as detailed in Section 2.2.2.

Carotid SNR was calculated differently. The DNN was used to generate predictions $\hat{E}'_m(n)$ for all $M = 6$ carotid channels. The peak finding was applied to $\hat{E}'_m(n)$ with the same contraints as previous. For every detected peak i in $\hat{E}'_m(n)$ at sample index

$n = \hat{p}_i^m$, an individual, bounded, SNR-based metric $\zeta_{m,i} \in [0, 1]$ is calculated as follows:

$$\zeta_{m,i} = \frac{\text{SNR}}{\text{SNR} + 1} = \frac{P_s^m}{P_s^m + P_v^m} \tag{13}$$

where P_s^m is now computed from $\hat{E}'_m(n)$ within a window spanning -2σ to $+2\sigma$ centered around $\hat{p}_i^m$. σ comes from the definition of $g(n)$, where a window of 4σ centered on the peak of the predicted Gaussian waveform should contain the predicted model output signal content if the model is correct. If the P_s^m is low, it highlights a poor prediction.

$$P_s^m = \sum_{n=\hat{p}_i^m-2\sigma}^{\hat{p}_i^m+2\sigma} \hat{E}'^2_m(n) \tag{14}$$

$\zeta_{m,i}$ was calculated on a segment of $\hat{E}'_m(n)$ around $\hat{p}_i^m$, as in (13) – (15).

The signal plus noise component $P_s + P_v$ is approximated as the energy of $E'(n)$ within a window between the previous and next peak locations. Specifically, denoting by $d_i^m = \hat{p}_{i+1}^m - \hat{p}_i^m$ the distance, in samples, between the current and next successive peak and analogously defining $d_{i-1} = \hat{p}_i^m - \hat{p}_{i-1}^m$, we define:

$$P_s^m + P_v^m = \sum_{n=\hat{p}_{i-1}^m+\frac{d_{i-1}}{2}}^{\hat{p}_i^m+\frac{d_i}{2}} \hat{E}'^2_m(n) \tag{15}$$

Note that due to heart rate variability, typically $d_{i-1}^m \neq d_i^m$. This process is visualized in Figure 6 for an example carotid signal of 20 seconds.

An average ζ_m is then calculated for each carotid channel: $\boldsymbol{\zeta} = \left[\zeta_1, \zeta_2, \ldots, \zeta_M\right]^T$.

$$\zeta_m = \frac{1}{\hat{I}} \sum \zeta_{m,i} \tag{16}$$

Where $\hat{I}$ denotes the number of detected heartbeat-related peaks within the considered segment of the model output. Specifically, $\hat{I}$ is computed over the entire length of signal $\hat{E}'_m(n)$. For instance, in panel B of Figure 6, we observe $\hat{I} = 23$.

For both the heart and carotid side, only channels with a ζ_m within one standard deviation of the maximum ζ_m were considered for further analysis because in those cases it can be reasonably expected that the model provided a relatively good prediction compared between the channels m. Only the $\hat{E}'_m(n)$ of the carotid channel with the maximum ζ_m was used for the segmentation of heart and carotid channels into epochs. It was empirically found that only the peaks with a $\zeta_{m,i} > 0.4$ in this channel were suitable for further processing. All included heart and carotid channels were segmented into individual epochs based on these detected peaks. Each heart channel was iteratively combined with each carotid channel.

At this point, the DNN-based *pseudo-ECG prediction* allowed us to detect heartbeat onsets, followed by carotid and heart signal segmentation. The next step towards

PTT calculation was designed to be similar to that described in section 2.3.1 for the template-matching method. Briefly, fiducial points had to be identified in the segmented epochs within physiologically sound windows. The signal features corresponding to the fiducial points are the same for this method, previously exemplified in Figure 2.

Taking the tolerance window for calculating Q_R into account (±30ms), slightly wider windows were used for this method as compared with those used for the template matching. This is because the model prediction is inherently less accurate as the ECG ground-truth. The fiducial points and window values are the same as for the ECG-dependent baseline method, outlined in section 2.2.2. The above steps are illustrated for one measurement in Figure 7. Pulse transit time (PTT) is subsequently estimated as described in Sections 2.2.2 and 2.3.1, by pairing fiducial points from the carotid (dicrotic notch) and cardiac (first inflection related to the second heart sound) signals that correspond to the same heartbeat and yield a physiologically plausible value.

A final difference between this method and the TM-based approach is the acceptance criterion for the final PTT. Here, if J is the total number of PTT estimates, the final PTT estimate is rejected if $J \leq \gamma N$, where N is the total sample length of the measured LDV signals. The threshold factor γ was set to 0.0025 (corresponding roughly to 50 PTT estimates over a 20-second segment. This threshold was chosen to be consistent with previous work with this LDV prototype, where this criterion yielded reliable results [23].

2.4 Experiments

Two separate databases were used (demographic data reported in Table 1). The first dataset, referred to as the CARDIS database, was collected as part of the CARDIS project [23]. CARDIS data were only used for the training, validation and testing datasets regarding the DNN-based method. It comprises data from 100 hypertensive subjects (age range: 23-73 years, 50% female). For each subject, three 20-second recordings were acquired under two measurement configurations: carotid–carotid (i.e., both laser Doppler vibrometry (LDV) handpieces mounted vertically and directed at the carotid artery) and carotid–femoral. This resulted in a total of 600 measurements, each containing six carotid signals, yielding a total of 3600 20-second carotid signals.

For this database, an expert previously visually scored all carotid signals on a 5-point scale ranging from 1 (very bad) to 5 (very good) [33]. 67 subjects had at least one measurement with at least one qualitative carotid channel (score 4 or 5) that could be included in the DNN training and evaluation process. Other data was discarded for the purpose of this study.

All signals of higher signal quality (visually scored 4 or 5 on the 5-pointer scale outlined in previous work [33]) were selected and segmented into $K = 9$ 50% overlapping segments of 4 seconds. The data pool was consequently split into 70 – 15 – 15 percent subsets for training, validation and test sets respectively.

Data leakage was strictly avoided by ensuring data from a subject were not simultaneously present in the training and the test/validation datasets. This protocol yielded 6055 4-second segments for the training set, 1431 segments for the validation set and 1432 segments for the test set. The training data was provided by 45 subjects. The

validation and testing data together entailed 22 subjects. Each segment had a corresponding reference ECG trace ($ECG(n)$), measured in parallel. These ECG traces served to generate the training targets as detailed in Section 2.3.2.

The second database (INSIDE) was generated during the H2020 InSiDe project (Grant agreement ID: 871547). This database was used to evaluate the PTT estimation methods, both ECG-based and ECG-free (template matching, DNN-based). Of importance for this work: 100 patients (age range: 18-81 years, 45% female) were included, each of whom had 3 heart-carotid measurements of varying lengths taken (with signal lengths of 10-60 seconds based on a minimum number of qualitative beats criterium [34]). One handpiece was pointed at the right common carotid artery, with the other pointed at the base of the heart i.e. the second right intercostal space, depicted in Figure 1.

PTT values for these data were previously estimated by manual segmentation based on $ECG(n)$, followed by a manual combination of fiducial points. This served as the reference for the benchmarking. The proposed heart-carotid PTT estimation method, using the DNN-based segmentation and SNR metrics, was assessed using this database. The previously proposed template-matching (TM) based method and automated ECG-based PTT estimation method were similarly evaluated on this database (see section 2.3.1 and 2.2.2 respectively).

For the DNN design, the INSIDE database was not called on during model training, validation and testing. Thus, it is completely unseen data. The skin acceleration data used across the two databases was resampled to a 1kHz sampling rate.

PTT estimates were computed for each individual LDV measurement in the INSIDE database that met the signal quality criteria, using ECG-based, template-matching based, and DNN-based methods. The resulting PTT arrays were individually correlated with the manual reference measurements to assess agreement. In addition, Bland–Altman analyses were performed to evaluate the level of concordance between each automated method and the manual reference. Statistical significance of the pairwise differences among the three automated methods was assessed using Wilcoxon signed-rank tests.

The CARDIS study was approved by the National Ethics Committee and the French National Drug Agency (ANSM) on 26.02.2018, Clinicaltrial.gov number: NCT03446430. The INSIDE study was approved by the National Ethics Committee and the French National Drug Agency (ANSM) on 28.11.2022, Clinicaltrial.gov number: NCT05711693. All methods were carried out in accordance with relevant guidelines and regulations. The authors have confirmed that any identifiable participants in this study have given their consent for publication. Informed consent of all participants in both studies was obtained. The datasets generated and/or analyzed during the current study are not publicly available due data management regulation of the InSiDe project but are available from the corresponding author on reasonable request.

InSiDe (N=100)		
Used for benchmarking the proposed methods (unseen data)		
Variable	Mean ± SD	Range
Age (years)	48 ± 17	[18, 81]
Sex (male %)	55	/
BMI (kg/m^2)	26 ± 5	[17.24, 39.82]
Systolic BP (mmHg)	130 ± 20	[88, 219]
Diastolic BP (mmHg)	79 ± 15	[49, 136]
Resting heart rate (bpm)	62 ± 11.33	[42, 97]
CARDIS (N=100)		
used for DNN model training, validation and testing		
Variable	Mean ± SD	Range
Age (years)	43 ± 19	[19, 85]
Sex (male %)	50	/
BMI (kg/m^2)	23 ± 3.6	[17.63, 31.6]
Systolic BP (mmHg)	118 ± 14.7	[96, 183]
Diastolic BP (mmHg)	64.5 ± 9.2	[45, 99]
Resting heart rate (bpm)	64 ± 8	[44, 89]

Table 1 Population statistics for both LDV databases. SD refers to standard deviation.

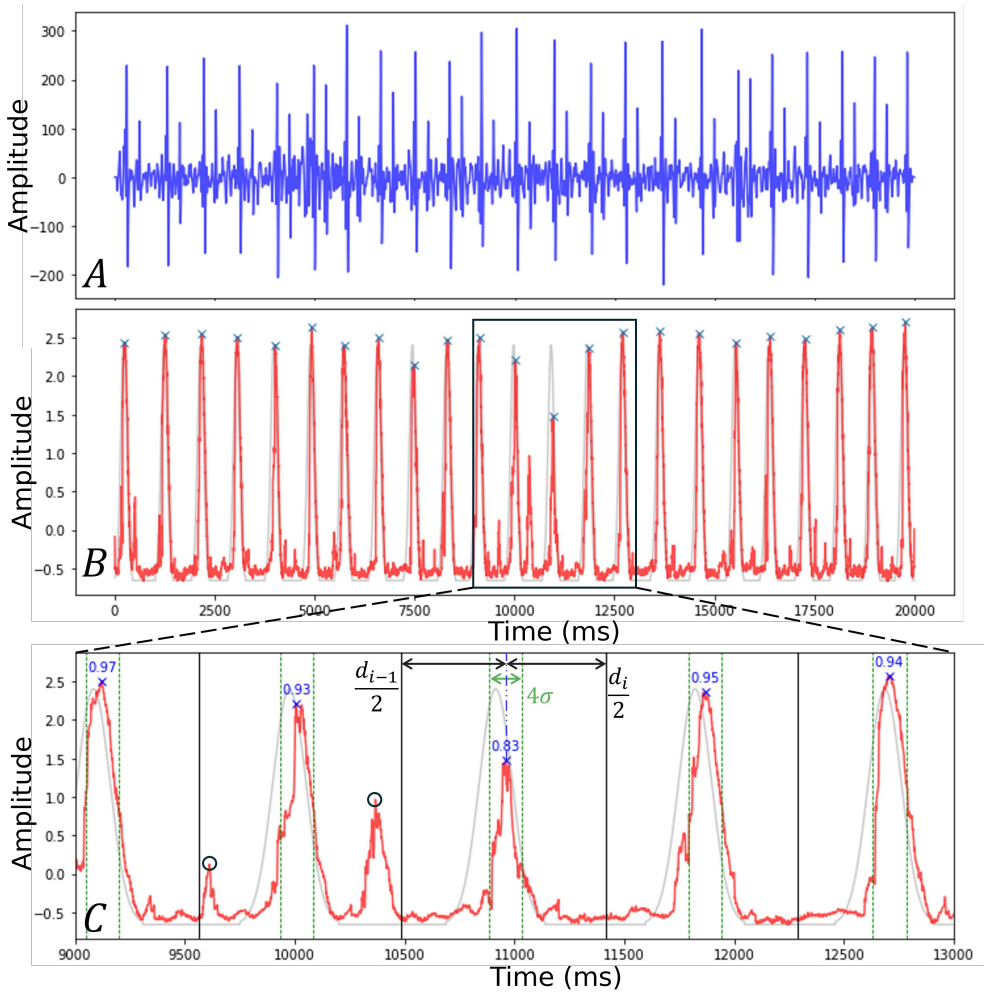


Fig. 6 Panel A: Example LDV carotid skin-acceleration signal contained in channel m of a measurement. Panel B: the model prediction $\hat{E}'_m(n)$ for the example signal. The ground truth $E'(n)$ is displayed for reference in gray in the background. Panel C: An illustrative segment of $\hat{E}'_m(n)$ is shown in which the detected beats are indicated. The individual peak SNR values $\zeta_{m,i}$ for the $\hat{I} = 23$ detected peaks are displayed, together with the boundaries within which the signal power P_s (vertical dashed line) and signal plus noise power $P_s + P_v$ (full vertical lines) are calculated. The gray graph is the corresponding $E'(n)$. This is shown to demonstrate that the ranges are selected appropriately. The two smaller peaks indicated with 'o' were excluded from the analysis based on the set criteria on amplitude and proximity to other peaks in time.

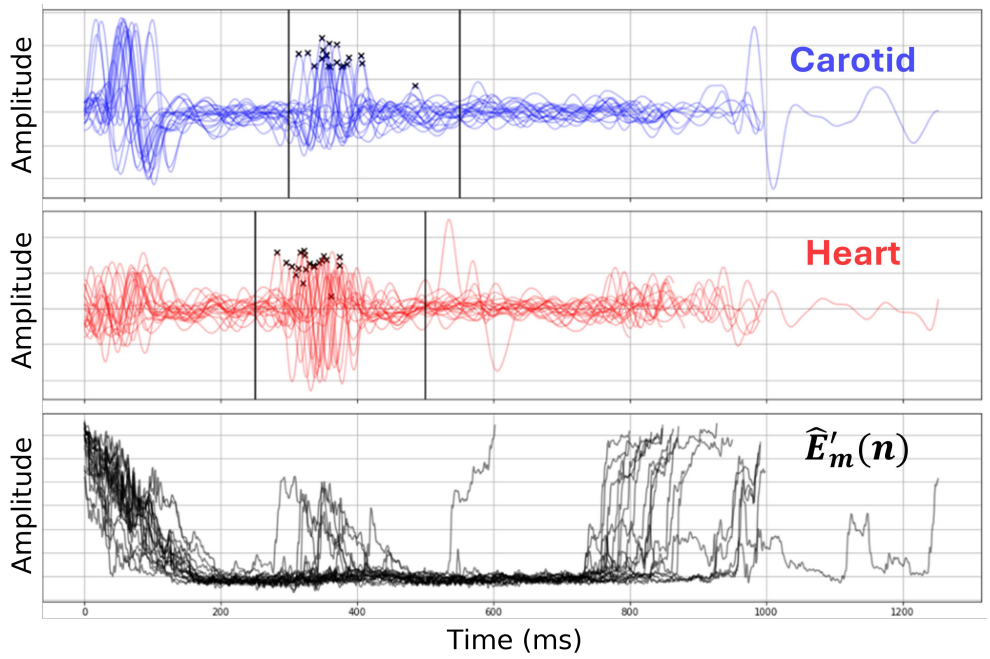


Fig. 7 Illustration of an example heart-carotid channel combination. Both channels were split into epochs according to the detected peaks in the preferred $\hat{E}'_m(n)$ (channel with highest ζ_m). The epoch-wise representation is given in the bottom plot. Carotid (top) and heart (middle) epochs are drawn together with the window limits between which the desired fiducial points are searched. Detected fiducial points are indicated with 'x'.

3 RESULTS

3.1 DNN validation

The performance of the DNN was first investigated through evaluation of the Q_R metric on every 4-second signal present in the validation and test sets. From visual inspection of the data, it was observed that signal quality varied, even between the selected higher-quality segments for the training, testing and validation sets [33]. There was also the presence of motion artifacts, potentially obscuring underlying heartbeat-related waveforms required by the DNN for an accurate prediction.

For the validation set, QRS detection scores had a median of 80% with an interquartile range (IQR) of 60–100%, and a mean of 77% with a 95% confidence interval (CI) of 75–78%. For the test set, the median score was 75% (IQR: 50–100%), with a mean of 69% (95% CI: 67–71%). This is visualized in Figure 8. The ratio of the total number of correctly detected beats in the model output and the total number of peaks in the target signals of the validation set was 77%. The same ratio for the test set was 68%.

The temporal distances between the timepoints of the predicted peaks in the model output and their corresponding reference peaks in the target signals were calculated for the validation and test set, resulting in the following statistics: In the validation set, the mean distance was 4.09 samples (95% CI: 3.71–4.47), with a median of 5.0 samples and an IQR spanning from –5.0 to 14.0 samples. The test set exhibited a mean distance of 6.22 samples (95% CI: 5.79–6.65), with a median of 7.0 samples and an IQR of –4.0 to 17.0 samples.

3.2 PTT estimation method performances

Following heartbeat onset detection using the DNN-based approach, the performance of PTT estimation was evaluated. Comparative results between the automated PTT methods and the manual reference are presented in Figure 9.

Panel A shows the results when the automated PTT algorithm using ground-truth ECG(n) for signal segmentation is utilized. A total of 201 datapoints stemming from 90 subjects are represented. Of the initial 300 data points, 12 were excluded due to measurement-procedure errors. These 12 datapoints were excluded for the analyses presented in panel B and C as well. An additional 87 were discarded owing to insufficient signal quality, which compromised fiducial point identification and PTT estimation. The correlation coefficient with the ground truth (manual PTT values) is $\rho = 0.69$, $p < 0.001$

Panel B shows the results for the template-matching based PTT method. Out of the 100 subjects included in the INSIDE study, for 46 subjects the method yielded a final PTT estimate from at least one of the three heart-carotid LDV measurements. In total, 78 measurements had a final result, as seen on the panel. Excluded from this analysis were 210 measurements due to the strict signal-quality criteria described in section 2.3.1. The correlation coefficient between the manual PTT and their corresponding automated PTT values is $\rho = 0.69$, $p < 0.001$.

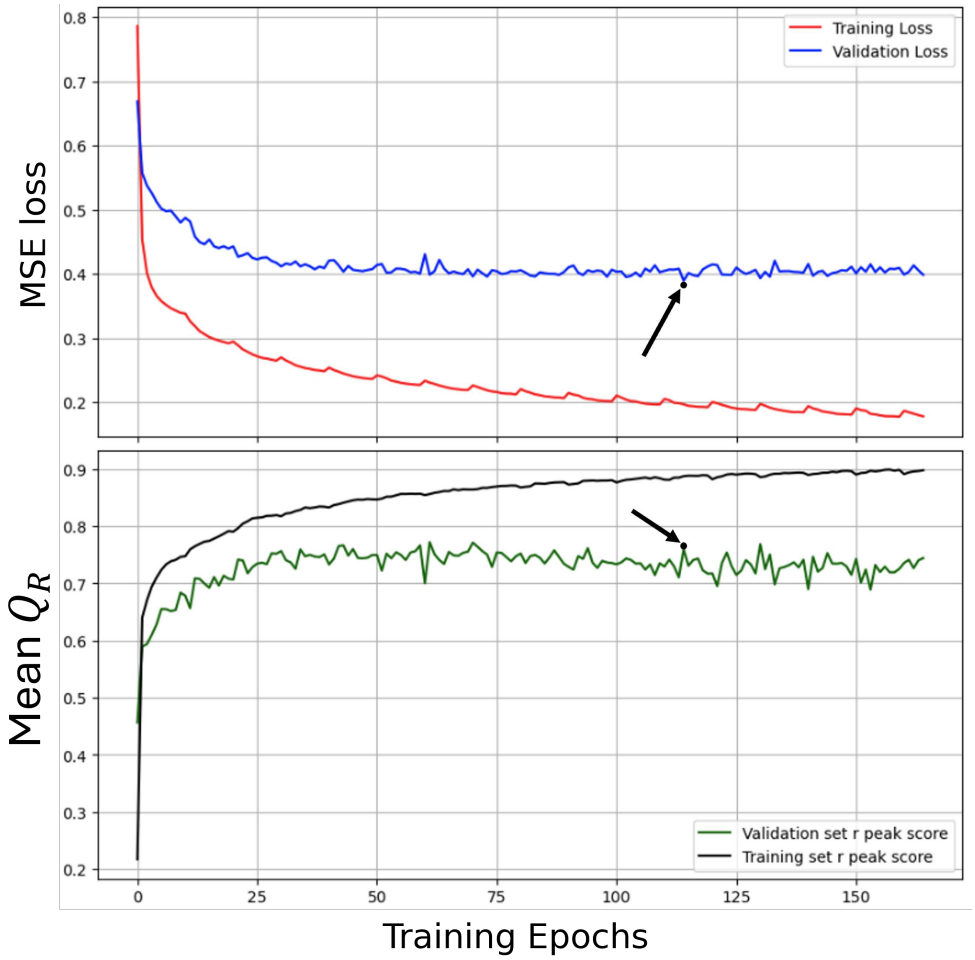


Fig. 8 Top panel: Training and validation as a function of training epochs. The training epoch at which the training process reached minimum MSE loss is indicated (training epoch 121). Bottom panel: R-peak score evolution during the DNN training for both training and validation sets.

Panel C in Figure 9 shows the datapoints of measurements with a final PTT value via the DNN-based method. These are plotted against and correlated with their corresponding manual PTT estimates. A total of 127 datapoints belonging to 64 INSIDE subjects were displayed. The signal-quality criteria built into the DNN-based method removed 161 measurements. A correlation coefficient of $\rho = 0.71$, $p < 0.001$ was found.

The Wilcoxon signed-rank test was employed to evaluate pairwise differences between automated PTT estimation methods. No statistically significant difference was observed between the ECG-based and TM-based approaches ($n = 62$, $W = 338.5$, $p = 0.64$; where W and n denote the Wilcoxon test statistic and number of paired observations respectively). Comparable results were obtained for the comparison

between ECG-based and DNN-based methods ($n = 110$, $W = 1262.5$, $p = 0.2965$), as well as between TM-based and DNN-based methods ($n = 66$, $W = 308$, $p = 0.11$).

Bland–Altman analyses were conducted to evaluate the agreement between each of the three automated PTT estimation methods and the manual reference. These analyses complement the correlation results and are presented in Figure 10.

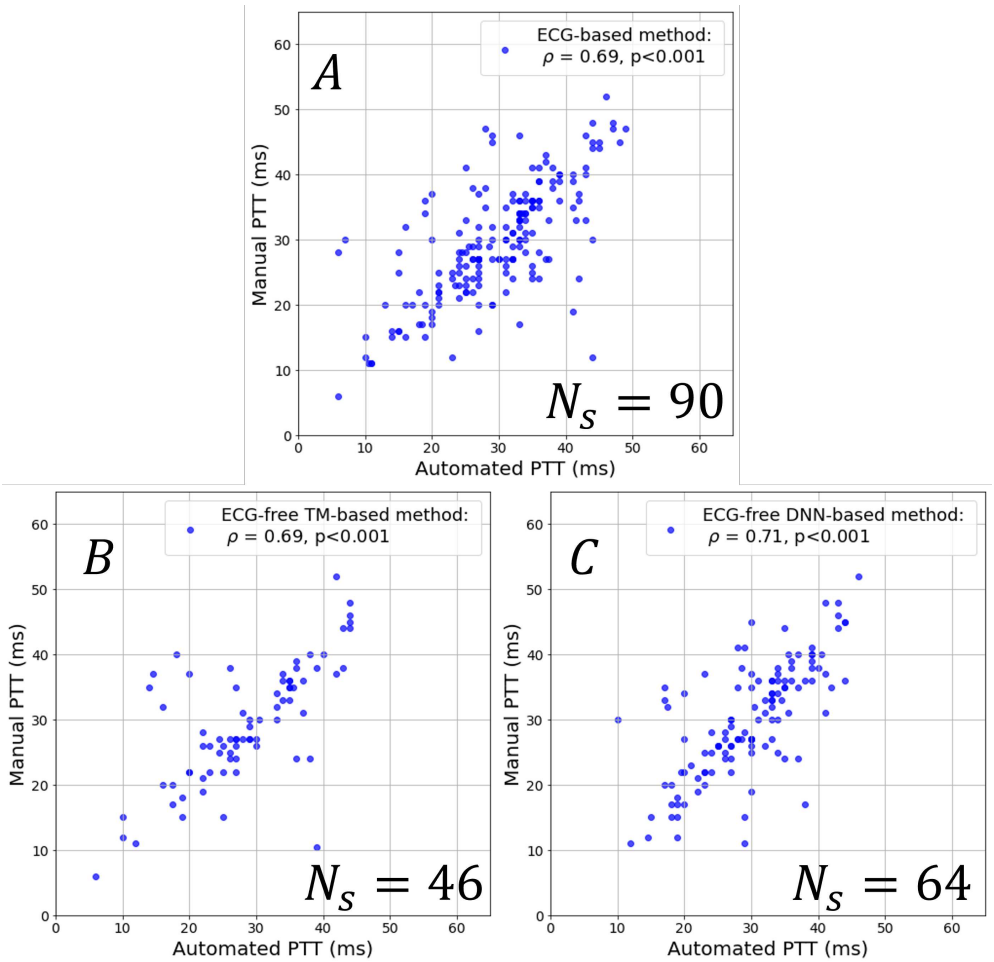


Fig. 9 Results comparing automated PTT estimates with manual PTT estimates. Panel A displays the ECG-based automated PTT estimates. Panel B shows template matching based, ECG-free automated PTT values and panel C shows those obtained using the ECG-free DNN-based $\hat{E}'(n)$ for segmentation. Correlation coefficients and corresponding p-values are indicated. N_S refers to the total number of unique subjects for whom a final PTT estimate was obtained by the corresponding methods.

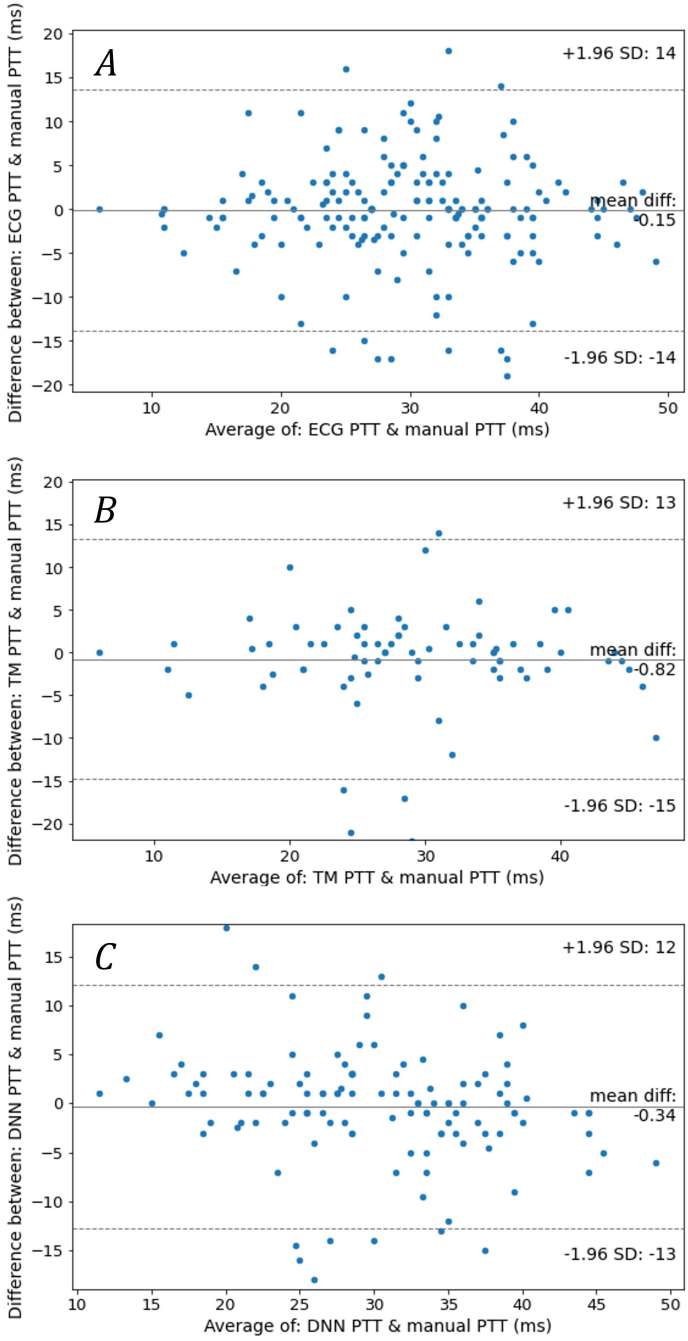


Fig. 10 Bland–Altman plots comparing automated PTT estimation methods with the manual reference values. Panel A displays ECG-based PTT values; Panels B and C show TM-based and DNN-based PTT values, respectively. 'SD' denotes standard deviation.

4 DISCUSSION

4.1 DNN-model validation for heartbeat onset prediction

The U-net inspired configuration was scaled in accordance with the prevalence of available training data. At 25k trainable parameters, the model is relatively small compared to e.g. the original Wave-U-Net model [55]. We did not observe overfitting i.e. the model training was halted before the observed validation loss (see Figure 8) increased in value after reaching its minimum.

Carotid signals were chosen as inputs to the model, instead of the heart-signals measured at the chest. Carotid LDV signals were better understood as the bulk of our earlier work investigated carotid-femoral measurements [22–24, 33]. Thus, selection of good quality data was deemed most feasible at the carotid site for this study.

The carotid signals also seemed to be more consistent in quality, demonstrating less pronounced effects on signal content from altered physiology due to cardiovascular disease. The signal-quality scores previously obtained per measured signal for the carotid signals in the CARDIS database allowed for selection of good to very good quality data [33], making the training, testing and validation data representative for the type of qualitative data that future applications of improved LDV-prototypes should provide.

Our application only required the detection of the onset of heartbeats in order to find fiducial points. R-waves in the $ECG(n)$ are critical for this and should be reliably predicted by the DNN for future LDV applications without the inclusion of ECG traces for experimental purposes. Therefore, a target signal containing information only on the timing of these R-waves is sufficient and simplifies the relation to be learnt between input and target signals.

Additionally, The conversion of raw ECG signals into a series of Gaussian pulses, denoted as $E'(n)$, proved beneficial for model performance. This transformation enabled training of the DNN using the straightforward and widely adopted mean squared error (MSE) loss function, which would be less effective with the sparse signal morphology characteristic of $ECG(n)$. The Gaussian filter parameter $\sigma = 75$ was empirically determined to offer a favorable trade-off between temporal precision and signal smoothness.

The R-peak score Q_R counts a correctly detected R-peak location in the model output $\hat{E}'(n)$ if it corresponds to an R-peak in the corresponding peak in the target signal $E'(n)$ within a 60 ms window centered on that R-peak. The validity of the Q_R metric is underscored by visual inspection of Figure 8, where the minimum value of the validation loss during training clearly corresponds to a maximum mean Q_R. A mean Q_R value of 69.1-76.8% and absolute heartbeat detection rates of 68.3-77.1% for unseen data (validation and test sets) indicates that our model performs reasonably well in detecting heartbeat onsets. We come to this conclusion considering the sensitivity of LDV data to motion artifacts.

We observed that the majority of the accepted R-peak locations in $\hat{E}'(n)$ do not perfectly coincide with the ground-truth peaks. On average, the model places a predicted heartbeat-onset peak slightly later than its reference. The reason why we accept these timeshifts (maximum of 30 ms before or after the ground-truth peak) is because

of the windowing in the later stages of PTT-estimation processing. The set windows, to locate the desired fiducial points, are wide enough to account for this margin of error. These windows also take into account the inter-subject variability in time between features such as the carotid foot of the wave and the dicrotic notch (the first and second peaks respectively in the signal in the middle plot of Figure 2).

It is important to note that a reliable PTT estimate does not require exhaustive processing of every single beat in a given measurement. Final DNN-based PTT estimates were accepted if e.g. for a $T_s = 20$ s signal, at least $J = 50$ PTT estimates were made across all considered channel combinations. Even if only $M = 3$ carotid and $M = 3$ heart channels pass their respective SNR criteria, this results in 9 channel combinations. Assuming a heart rhythm of 60 bpm (a realistic lower bound), with 20 beats in the T_s measurement. Taking the lower absolute heartbeat detection rate of 68.3% on DNN output, this would mean that 13 of the 20 heartbeats in the signal are detected. This leads to $9 \times 13 = 117$ total beat-pairs considered for PTT calculation, which passes the constraint of at least 50 PTT estimates, given the signal length, implying that the DNN-based method can return reliable PTT values based on a smaller subset of the available data from one LDV measurement.

4.2 TM- vs DNN-Based PTT Estimation

As shown in panel A of Figure 9, segmentation based on the raw ECG signal yields acceptable PTT estimates for the majority of subjects. This approach would be the most inclusive, assuming ECG could be readily acquired alongside LDV. However, such integration is unlikely in any future commercially viable LDV systems designed for non-invasive cardiovascular monitoring.

Outliers are evident across all three methods, as illustrated in Figure 10, despite minimal bias (i.e., low mean difference values) between automated and manual estimates. The limits of agreement are comparably wide across methods. Although minor differences in correlation coefficients are observed, the Wilcoxon signed-rank tests indicate that differences between the methods are not statistically significant. Therefore, the primary consideration when selecting between the TM-based and DNN-based approaches is their relative inclusivity, specifically the number of subjects for whom a reliable PTT estimate can be obtained.

The TM-based method applied stringent signal-quality criteria to ensure reliable PTT estimation. While these safeguards improved result fidelity, they also led to the exclusion of a substantial number of measurements, ultimately yielding valid results for only 46 subjects, highlighting a key limitation of this approach.

The DNN-based method employed comparable quality thresholds for both input signals and model output. Under these conditions, it produced valid PTT estimates for 64 subjects. This outcome suggests that the DNN approach demonstrates good agreement with the reference method and, importantly, offers greater inclusivity. Its broader applicability in practical settings, particularly where signal quality may vary, is a notable advantage.

The discrepancy in subject inclusion between the TM-based and DNN-based PTT estimation methods is not because of more measurement exclusion in TM. It can be partially explained by the example shown in Figure 11. This figure presents a

segment of carotid LDV data characterized by low signal quality—specifically, diminished signal-to-noise ratio and physiologically relevant peaks that are less distinct and morphologically atypical. In this instance, the TM algorithm identified matches and attempted to detect the carotid foot, but failed to correctly localize the waveform features. In contrast, the DNN-generated $\hat{E}'(n)$ for the same segment, while not flawless, placed peaks in reasonable temporal proximity to the automatically detected ECG R-peaks. This example reflects a broader trend observed across the dataset: the TM method is more vulnerable to signal degradation, whereas the DNN demonstrates greater resilience, underscoring the advantage of data-driven representations in handling variable signal quality.

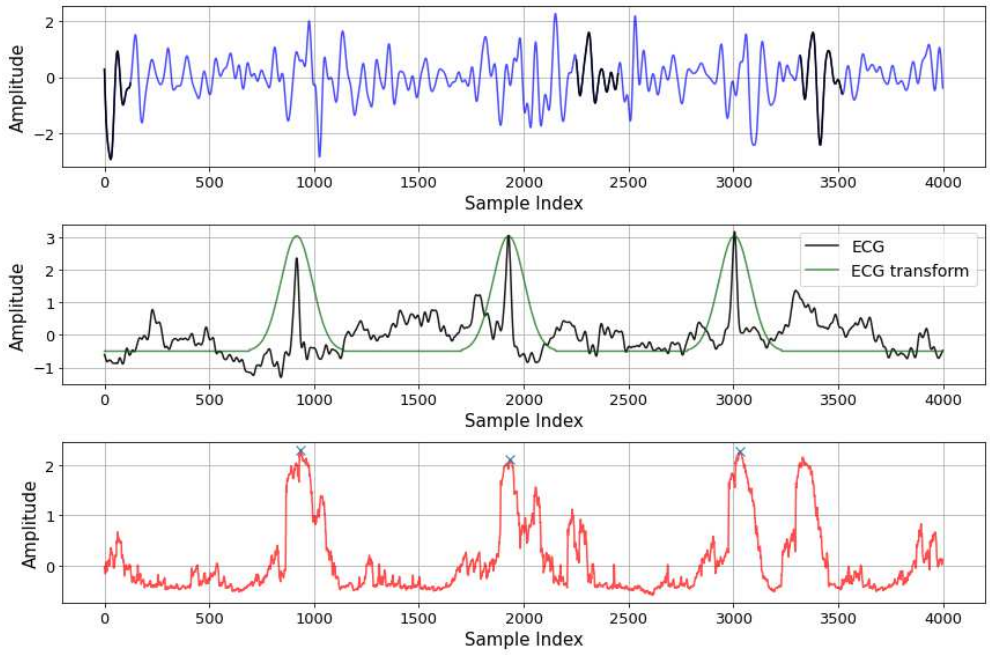


Fig. 11 An example of a low-quality carotid signal (blue) and its corresponding ECG (black, second panel). Indicated in black on the first panel are the waveforms in the LDV signal that were identified by template matching. The detected waveforms do not correspond with actual heartbeats here. DNN output is shown in red, in which detected peaks are marked. These peaks do correspond with heartbeat onsets as can be seen from the R peaks in the ECG signal, leading to an acceptable PTT estimate.

4.3 Future Applications

All measurements in both CARDIS and InSiDe studies were conducted using the CARDIS prototype. This device has a few drawbacks. Namely, it requires the application of retroreflective tape on the measurement site to ensure ample reflection of the incident laser beams. This requirement likely influences the signal content and quality, and can only be addressed through hardware improvements that eliminate the need for surface preparation. Within the scope of the InSiDe project, a next-generation LDV prototype is under development to overcome this constraint and thereby potentially improve measurement signal quality. With this, the DNN could be expanded with larger, more qualitative LDV databases to be more accurate and representative.

Other project objectives for InSiDe are the development of algorithms for estimating carotid-femoral pulse-wave velocity, investigating carotid stenosis and cardiac arrythmia [25, 26, 58]. For the latter especially, but not exclusively, the DNN could prove useful as its output contains information on the heartbeat onset timing within a given measurement. One could generalize the potential use of the DNN to any cardiac application of LDV, potentially even for non-carotid signals (given a retraining of the DNN on e.g. heart or femoral artery LDV measurements).

4.4 Remaining Challenges

Given the relative niche application of LDV within the current state of the art and especially the paucity of other studies investigating heart-carotid PTT, there is little literature to compare the results of this work to.

5 CONCLUSION

A DNN was trained for the purpose of heartbeat onset prediction in LDV signals measured at the carotid artery. The model training was done by way of a transformation applied to raw ECG signals that were measured in parallel with the LDV signals. This transformation consisted of Gaussian pulses at the location of the ECG R peaks, conserving only information of their timing and facilitating a simplified MSE loss-function application. Leveraging the DNN's output, signal segmentation becomes feasible even in the absence of ground-truth ECG, which will be absent from future medical LDV implementations. From the segmented heartbeats, fiducial points were identified which led to heart-carotid PTT values. This DNN-based method lead to heart-carotid PTT estimates which showed comparable correlation with reference PTT values to those obtained via TM-based and ECG-dependent methods. The DNN method, however, yielded results for significantly more subjects than TM. We conclude that the DNN method provides added value in the form of a proxy for the ECG, leading to robust heartbeat segmentation in the absence of a measured ECG signal.

Acknowledgements

All work done in this article, was performed within the scope of the H2020-project: InSiDe (Grant agreement ID: 871547).

The author's have confirmed that any identifiable participants in this study have given their consent for publication.

Ethical Statement

The InSide study was approved by the National Ethics Committee and the French National Drug Agency (ANSM) on 28.11.2022, Clinicaltrial.gov number: NCT05711693.

The CARDIS study was approved by the National Ethics Committee and the French National Drug Agency (ANSM) on 26.02.2018, Clinicaltrial.gov number: NCT03446430.

Funding Declaration

Funding for the work represented in this work was provided by the H2020 Industrial Leadership grant (ID: 871547).

References

[1] Wolinsky, H., Glagov, S.: A lamellar unit of aortic medial structure and function in mammals. Circulation Research **20**, 99–111 (1967)

[2] Westerhof, N., Lankhaar, J.-W., Westerhof, B.E.: The arterial windkessel. Medical & biological engineering & computing **47**(2), 131–141 (2009) https://doi.org/10.1007/s11517-008-0359-2

[3] Parker, K.H.: A brief history of arterial wave mechanics. Med. Biol. Eng. Comput. **47**(2), 111–118 (2009)

[4] Chirinos, J.A., Segers, P., Hughes, T., Townsend, R.: Large-artery stiffness in health and disease: JACC state-of-the-art review. Journal American College of Cardiology **74**(9), 1237–1263 (2019) https://doi.org/10.1016/j.jacc.2019.07.012

[5] Vlachopoulos, C., Aznaouridis, K., Stefanadis, C.: Prediction of cardiovascular events and all-cause mortality with arterial stiffness: A systematic review and meta-analysis. Journal of the American College of Cardiology **55**(13), 1318–1327 (2010) https://doi.org/10.1016/j.jacc.2009.10.061

[6] Laurent, S., Cockcroft, J., Van Bortel, L., Boutouyrie, P., Giannattasio, C., Hayoz, D., Pannier, B., Vlachopoulos, C., Wilkinson, I., Struijker-Boudier, H.: Expert consensus document on arterial stiffness: methodological issues and clinical applications. European Heart Journal **27**(21), 2588–2605 (2006)

[7] Ben-Shlomo, Y., Spears, M., Boustred, C., May, M., Anderson, S.G., Benjamin, E.J., Boutouyrie, P., Cameron, J., Chen, C., Cruickshank, J.K., Hwang, S., Lakatta, E.G., Laurent, S., Maldonado, J., Mitchell, G.F., Najjar, S.S., Newman, A.B., Ohishi, M., Pannier, B., Pereira, T., Vasan, R.S., Shokawa, T.,

Sutton-Tyrell, K., Verbeke, F., Wang, K., Webb, D.J., H., W., Zoungas, S., McEniery, C.M., Cockcroft, J.R., Wilkinson, I.B.: Aortic pulse wave velocity improves cardiovascular event prediction. J. Am. Coll. Cardiol. **63**(7), 636–646 (2014)

[8] Alastruey, J., Charlton, P.H., Bikia, V., Paliakaite, B., Hametner, B., Bruno, R.M., Mulder, M.P., Vennin, S., Piskin, S., Khir, A.W., Guala, A., Mayer, C.C., Mynard, J., Hughes, A.D., Segers, P., Westerhof, B.E.: Arterial pulse wave modeling and analysis for vascular-age studies: a review from VascAgeNet. Am. J. Physiol. Heart Circ. Physiol. **325**(1), 1–29 (2023)

[9] Mitchell, G.F., Hwang, S., Vasan, R.S., Larson, M.G., Pencina, M.J., Hamburg, N.M., Vita, J.A., Levy, D., Benjamin, E.J.: Arterial stiffness and cardiovascular events: the framingham heart study. Circulation **121**(4), 505–511 (2010)

[10] Segers, P., Rietzschel, E.R., Chirinos, J.A.: How to measure arterial stiffness in humans. Arteriosclerosis, thrombosis, and vascular biology **40**(5), 1034–1043 (2020)

[11] Boutouyrie, P., Bruno, R.M.: The clinical significance and application of vascular stiffness measurements. Am. J. Hypertens. **32**(1), 4–11 (2019)

[12] Pereira, T., Correia, C., Cardoso, J.: Novel methods for pulse wave velocity measurement. Journal of medical and biological engineering **35**(5), 555–565 (2015)

[13] Kim, W.Y., Astrup, A.S., Stuber, M., Tarnow, L., Falk, E., Botnar, R.M., Simonsen, C., Pietraszek, L., Hansen, P.R., Manning, W.J., Andersen, N.T., Parving, H.: Subclinical coronary and aortic atherosclerosis detected by magnetic resonance imaging in type 1 diabetes with and without diabetic nephropathy. Circulation **115**(2), 228–235 (2007)

[14] Elderen, S.G.C., Brandts, A., Westenberg, J.J.M., Grond, J., Tamsma, J.T., Buchem, M.A., Romijn, J.A., Kroft, L.J.M., Smit, J.W.A., Roos, A.: Aortic stiffness is associated with cardiac function and cerebral small vessel disease in patients with type 1 diabetes mellitus: assessment by magnetic resonance imaging. Eur. Radiol. **20**(5), 1132–1138 (2010)

[15] Brandts, A., Elderen, S.G.C., Tamsma, J.T., Smit, J.W.A., Kroft, L.J.M., Lamb, H.J., Meer, R.W., Westenberg, J.J.M., Roos, A.: The effect of hypertension on aortic pulse wave velocity in type-1 diabetes mellitus patients: assessment with MRI. Int. J. Cardiovasc. Imaging **28**(3), 543–550 (2012)

[16] Cawley, C., McEvoy, J.W.: European guidelines for risk assessment in the primary prevention of cardiovascular disease. In: Contemporary Cardiology, pp. 35–58. Springer, Cham (2022)

[17] Melis, M.D., Morbiducci, U., Scalise, L., Tomasini, E.P., Delbeke, D., Baets, R.,

Bortel, L.M.V., Segers, P.: A noncontact approach for the evaluation of large artery stiffness: a preliminary study. American journal of hypertension **21**(12), 1280–1283 (2008)

[18] Campo, A., Dirckx, J.: Dual-beam laser doppler vibrometer for measurement of pulse wave velocity in elastic vessels. In: 22nd Congress Intl. Commission for Optics: Light for the Development of the World, vol. 8011, p. 80118 (2011). International Society for Optics and Photonics

[19] Kaplan, A.D., O'Sullivan, J.A., Sirevaag, E.J., Lai, P.-H., Rohrbaugh, J.W.: Hidden state models for noncontact measurements of the carotid pulse using a laser doppler vibrometer. IEEE Transactions on Biomedical Engineering **59**(3), 744–753 (2012) https://doi.org/10.1109/tbme.2011.2179297

[20] Morbiducci, U., Scalise, L., Melis, M.D., Grigioni, M.: Optical vibrocardiography: A novel tool for the optical monitoring of cardiac activity. Annals Biomedical Engg. **35**(1), 45–58 (2007)

[21] Li, Y., Segers, P., Dirckx, J., Baets, R.: On-chip laser doppler vibrometer for arterial pulse wave velocity measurement. Biomedical optics express **4**(7), 1229–1235 (2013)

[22] Li, Y., Marais, L., Khettab, H., Quan, Z., Aasmul, S., Leinders, R., Schüler, R., Morrissey, P.E., Greenwald, S., Segers ,*et al*, P.: Silicon photonics-based laser doppler vibrometer array for carotid-femoral pulse wave velocity (PWV) measurement. Biomedical Optics Express **11**(7), 3913–3926 (2020)

[23] Badhwar, S., Marais, L., Khettab, H., Poli, F., Li, Y., Segers, P., Aasmul, S., Melis, M., Baets, R., Greenwald, S., Bruno, R.M., Boutouyrie, P.: Clinical validation of carotid-femoral pulse wave velocity measurement using a multi-beam laser vibrometer: The CARDIS study. Hypertension **81**(9), 1986–1995 (2024)

[24] Marais, L., Khettab, H., Li, Y., Segers, P., Baets, R., Reesink, K., Aasmul, S., De Melis, M., Boutouyrie, P.: Measurement of aortic stiffness by laser doppler vibrometry: The CARDIS study. Journal of Hypertension **37**, 88 (2019)

[25] Mancini, V., Tommasin, D., Li, Y., Reeves, J., Baets, R., Greenwald, S., Segers, P., CARDIS consortium: Detecting carotid stenosis from skin vibrations using laser doppler vibrometry - an in vitro proof-of-concept. PLoS One **14**(6), 0218317 (2019)

[26] Mancini, V. and Bergersen, A. W. and Valen-Sendstad, K. and Segers, P.: Computed poststenotic flow instabilities correlate phenotypically with vibrations measured using laser Doppler vibrometry : perspectives for a promising in vivo device for early detection of moderate and severe carotid stenosis. JOURNAL OF BIOMECHANICAL ENGINEERING-TRANSACTIONS OF THE ASME **142**(9), 13 (2020)

[27] Li, C., Xiong, H., Pirbhulal, S., Wu, D., Li, Z., Huang, W., Zhang, H., Wu, W.: Heart-carotid pulse wave velocity a useful index of atherosclerosis in chinese hypertensive patients. Medicine (Baltimore) **94**(51), 2343 (2015)

[28] Faita, F., Gemignani, V., Bianchini, E., Bruno, R.M., Bombardini, T., Ghiadoni, L.: P9.04 a new method for continuous monitoring of central arterial stiffness during stress. Artery Res. **3**(4), 167 (2009)

[29] Beeckman, S., Badhwar, S., Li, Y., Aasmul, S., Madhu, N., Khettab, H., Mousseaux, E., Gencer, U., Boutouyrie, P., Bruno, R.M., Segers, P.: Heart-carotid pulse-wave velocity via laser-doppler vibrometry as a biomarker for arterial stiffening: a feasibility study. Physiol. Meas. (2025)

[30] Won-Du, C., Chang-Hwan, I.: Enhanced Template Matching Using Dynamic Positional Warping for Identification of Specific Patterns in Electroencephalogram. Journal of Applied Mathematics **2014** (2014)

[31] Shinichiro, O., Masako, O.: Fast Template Matching With Polynomials. IEEE TRANSACTIONS ON IMAGE PROCESSING **16**(8) (2007)

[32] Jiun-Hung, C., Chu-Song, C., Yong-Sheng, C.: Fast Algorithm for Robust Template Matching With M-Estimators. IEEE TRANSACTIONS ON SIGNAL PROCESSING **51**(1) (2003)

[33] Seoni, S., Beeckman, S., Li, Y., Aasmul, S., Morbiducci, U., Baets, R., Boutouyrie, P., Molinari, F., Madhu, N., Segers, P.: Template matching and matrix profile for signal quality assessment of carotid and femoral laser doppler vibrometer signals. Frontiers in Physiology **12** (2022)

[34] Seoni, S., Segers, P., Beeckman, S., Salvi, M., Romanelli, M., Badhwar, S., Bruno, R.M., Li, Y., Aasmul, S., Madhu, N., Molinari, F., Morbiducci, U.: Real-time beat-to-beat pulse wave velocity estimation: a quality-driven approach using laser doppler vibrometry. Med. Biol. Eng. Comput. (2025)

[35] Yao, J., Tridandapani, S., Auffermann, W.F., Wick, C.A., Bhatti, P.T.: An adaptive seismocardiography (SCG)-ECG multimodal framework for cardiac gating using artificial neural networks. IEEE J. Transl. Eng. Health Med. **6**, 1900611 (2018)

[36] Nikbakht, M., Gazi, A.H., Zia, J., An, S., Lin, D.J., Inan, O.T., Kamaleswaran, R.: Synthetic seismocardiogram generation using a transformer-based neural network. J. Am. Med. Inform. Assoc. **30**(7), 1266–1273 (2023)

[37] Pourbabaee, B., Roshtkhari, M.J., Khorasani, K.: Deep convolutional neural networks and learning ECG features for screening paroxysmal atrial fibrillation patients. IEEE Trans. Syst. Man Cybern. Syst. **48**(12), 2095–2104 (2018)

[38] Acharya, U.R., Fujita, H., Oh, S.L., Hagiwara, Y., Tan, J.H., Adam, M.: Application of deep convolutional neural network for automated detection of myocardial infarction using ECG signals. Inf. Sci. (Ny) **415-416**, 190–198 (2017)

[39] Rajwal, S., Aggarwal, S.: Convolutional neural network-based EEG signal analysis: A systematic review. Arch. Comput. Methods Eng. (2023)

[40] Jiang, Y., Yao, T., Paliwal, N., Knight, D., Punjabi, K., Steeden, J., Hughes, A.D., Muthurangu, V., Davies, R.: Fully automated measurement of aortic pulse wave velocity from routine cardiac MRI studies. Magn. Reson. Imaging **122**(110442), 110442 (2025)

[41] Zheng, Y., Wu, C., Cai, P., Zhong, Z., Huang, H., Jiang, Y.: Tiny-PPG: A lightweight deep neural network for real-time detection of motion artifacts in photoplethysmogram signals on edge devices. Internet of Things **25**(101007), 101007 (2024)

[42] Habib, A., Motin, M.A., Penzel, T., Palaniswami, M., Yearwood, J., Karmakar, C.: Performance of a convolutional neural network derived from PPG signal in classifying sleep stages. IEEE Trans. Biomed. Eng. **70**(6), 1717–1728 (2023)

[43] El-Hajj, C., Kyriacou, P.A.: A review of machine learning techniques in photoplethysmography for the non-invasive cuff-less measurement of blood pressure. Biomed. Signal Process. Control **58**(101870), 101870 (2020)

[44] Abrisham, K.P., Alipour, K., Tarvirdizadeh, B., Ghamari, M.: Deep learning-based estimation of arterial stiffness from PPG spectrograms: A novel approach for non-invasive cardiovascular diagnostics. Annu. Int. Conf. IEEE Eng. Med. Biol. Soc. **2024**, 1–7 (2024)

[45] Faust, O., Hagiwara, Y., Hong, T.J., Lih, O.S., Acharya, U.R.: Deep learning for healthcare applications based on physiological signals: A review. Comput. Methods Programs Biomed. **161**, 1–13 (2018)

[46] Bozkurt, B., Germanakis, I., Stylianou, Y.: A study of time-frequency features for CNN-based automatic heart sound classification for pathology detection. Comput. Biol. Med. **100**, 132–143 (2018)

[47] Meintjes, A., Lowe, A., Legget, M.: Fundamental heart sound classification using the continuous wavelet transform and convolutional neural networks. In: 2018 40th Annual International Conference of the IEEE Engineering in Medicine and Biology Society (EMBC), pp. 409–412 (2018). IEEE

[48] Khan, J.S., Kaushik, M., Chaurasia, A., Dutta, M.K., Burget, R.: Cardi-Net: A deep neural network for classification of cardiac disease using phonocardiogram signal. Comput. Methods Programs Biomed. **219**(106727), 106727 (2022)

[49] Gamilov, T., Liang, F., Kopylov, P., Kuznetsova, N., Rogov, A., Simakov, S.: Computational analysis of hemodynamic indices based on personalized identification of aortic pulse wave velocity by a neural network. Mathematics **11**(6), 1358 (2023)

[50] Hout, M.J., Dekkers, I.A., Lin, L., Westenberg, J.J., Schalij, M.J., Jukema, J.W., Widya, R.L., Boone, S.C., Mutsert, R., Rosendaal, F.R., Scholte, A.J., Lamb, H.J.: Estimated pulse wave velocity (ePWV) as a potential gatekeeper for MRI-assessed PWV: a linear and deep neural network based approach in 2254 participants of the netherlands epidemiology of obesity study. Int. J. Cardiovasc. Imaging **38**(1), 183–193 (2022)

[51] Alhakak, A.S., Olsen, F.J., Skaarup, K.G., Lassen, M.C.H., Johansen, N.D., Espersen, C., Abildgaard, U., Jensen, G.B., Schnohr, P., Marott, J.L., Søgaard, P., Møgelvang, R., Biering-Sørensen, T.: Changes in cardiac time intervals over a decade and the risk of incident heart failure: The copenhagen city heart study. Int. J. Cardiol. **386**, 141–148 (2023)

[52] Biering-Sørensen, T., Mogelvang, R., Knegt, M.C., Olsen, F.J., Galatius, S., Jensen, J.S.: Cardiac time intervals by tissue doppler imaging m-mode: Normal values and association with established echocardiographic and invasive measures of systolic and diastolic function. PLoS One **11**(4), 0153636 (2016)

[53] Beeckman, S., Li, Y., Aasmul, S., Baets, R., Boutouyrie, P., Segers, P., Madhu, N.: Enhancing multichannel laser-doppler vibrometry signals with application to (carotid-femoral) pulse transit time estimation. Annu. Int. Conf. IEEE Eng. Med. Biol. Soc. **2023**, 1–7 (2023)

[54] Ronneberger, O., Fischer, P., Brox, T.: U-net: Convolutional networks for biomedical image segmentation. In: Medical Image Computing and Computer-Assisted Intervention (MICCAI). LNCS, vol. 9351, pp. 234–241. Springer, ??? (2015). http://lmb.informatik.uni-freiburg.de/Publications/2015/RFB15a

[55] Stoller, D., Ewert, S., Dixon, S.: Wave-U-Net: A multi-scale neural network for end-to-end audio source separation. arXiv [cs.SD] (2018) [cs.SD]

[56] Petit, O., Thome, N., Rambour, C., Themyr, L., Collins, T., Soler, L.: U-Net transformer: Self and cross attention for medical image segmentation. In: Machine Learning in Medical Imaging. Lecture notes in computer science, pp. 267–276. Springer, Cham (2021)

[57] Mu, N., Yao, Z., Gholami, A., Keutzer, K., Mahoney, M.: Parameter re-initialization through cyclical batch size schedules. arXiv [cs.LG] (2018) [cs.LG]

[58] Mancini, V., Bergersen, A.W., Vierendeels, J., Segers, P., Valen-Sendstad, K.: High-frequency fluctuations in post-stenotic patient specific carotid stenosis fluid dynamics: A computational fluid dynamics strategy study. Cardiovasc. Eng.

Technol. **10**(2), 277–298 (2019)